UNIVERSIDADE FEDERAL DO RIO GRANDE DO SUL
ESCOLA DE ENGENHARIA
TRABALHO DE CONCLUSÃO EM ENGENHARIA DE CONTROLE E AUTOMAÇÃO

Evaluation of Altitude Sensors for an Application in a Pulverization Drone

Author: Matheus Hentschke

Advisor: Edison Pignaton de Freitas

Porto Alegre, December 22, 2017

Contents

Acknowledgments

My sincere acknowledgments

To my advisor, Professor Edison Pignaton de Freitas for providing unique opportunities of professional and personal growth and for encouraging me to follow the research path which brought me many realizations.

To Lascar's team for the help and incentive provided.

To Skydrones Tecnologia Aviônica S/A for providing the materials, resources and experienced professionals necessary for this research.

To Skydrones' team for the help provided and encouragement for the execution of this work.

To my parents for the constant support and encouragement, as well as the love, dedication and comprehension. Their knowledge and always present guidance were crucial to my trajectory.

To my sister for all the advise and knowledge passed, as well as the company at home and the help with this work.

To my girlfriend Marceli for the love, attention, dedication, good humor, comprehension and support, present even at distance. The happy moments were special and essential to my success.

To my university friends Bruna Ramos, Henrique Pinheiro, Igor da Veiga, Lucas Muratore, Maria Cristina Kopacek and Mauricio Farina for the countless happy moments and also for the support during the bad ones.

To my older friends Haran Camatti, Raphael Zaneti and Thiago Spiringer for making my growing up process much better and happier.

Abstract

This work aims to study and compare various range finders applied to altitude sensing on a rotating wings Unmanned Aerial Vehicle (UAV). The specific application is the altitude maintenance for the fluid deployment valve aperture control in an unmanned pulverization aircraft used in precision agriculture. The influence of a variety of parameters will be analyzed, including the tolerance for crop inconsistencies, density variations and intrinsic factors to the process, such as the pulverization fluid interference in the sensor's readings, as well as their vulnerability to harsh conditions of the operation environment. Filtering and data extraction techniques were applied and analyzed in order to potentiate the measurement reliability. As a result, a wide study was produced, enabling the better decision making about choosing the best sensor for each situation being analyzed. The performed data analysis was able to provide a reliable baseline to which the sensors could be compared. With a baseline set, it was possible to counterweigh the sensors errors and other measures like the Mean Squared Error (MSE) for each environment to provide a summarized score of the sensors in order to support product design decision making. The sensors which provided the best performance in the metrics used were Lightware SF11-C and LeddarTech M16, according to the environment.

Resumo

Este trabalho tem como finalidade o estudo e a comparação entre diversos sensores de alcance aplicados à determinação de altitude de um *Veículo Aéreo Não Tripulado* (VANT) de asas rotativas. A aplicação específica é a de manutenção de altitude para o controle de abertura da válvula de liberação de fluido para uma aeronave não tripulada com o propósito de pulverização no contexto de agricultura de precisão. São analisadas as influências de diversos tipos de parâmetros nas leituras dos sensores, incluindo tolerância a falhas dependendo de características da plantação e variações na densidade da mesma, além de sua tolerância a fatores intrínsecos ao processo como a interferência do fluido sendo pulverizado nas leituras dos sensores, assim como a vulnerabilidade dos sensores às condições agressivas do ambiente em que os mesmos operam. São, ainda, realizadas análises de forma a determinar os efeitos benéficos ou não de técnicas de filtragem e extração de dados dos sinais obtidos de forma a potencializar os resultados obtidos a partir dos sensores. Como resultado, obtém-se um estudo abrangente de forma a possibilitar o embasamento da escolha do melhor sensor para cada situação analisada. A análise dos dados possibilitou a obtenção te uma referência confiável à qual é possível comparar os sensores individuais. Com uma referência fixada, foi possível comparar os erros dos sensores e outras medidas como o MSE para cada um dos ambientes de forma a obter uma pontuação que resume a qualidade de medida do sensor, possibilitando uma tomada de decisão de projeto embasada. Os sensores que geraram os melhores resultados nas métricas utilizadas foram o Lightware SF11-C e o LeddarTech M16, sendo que o melhor sensor varia de caso a caso

List of Figures

List of Tables

List of Abbreviations

ADC	Analog-Digital Converter. 5
AGL	Height Above Ground Level. 1, 2
AI	Artificial Intelligence. 17
AMSL	Height Above Mean Sea Level. 2
CAD	Computer Aided Design. 12
CAM	Computer Aided Manufacturing. 12
CLI	Command Line Interface. 15
CNC	Computer Numeric Control. 12
COTS	Commercial-Off-The-Shelf. 9
CPU	Central Processing Unit. 9, 12
CSV	Comma-separated values. v, 14, 15
DOF	Degrees of Freedom. 16
DSP	Digital Signal Processor. 5
DTFT	Discrete Time Fourier Transform. 7
FFT	Fast Fourier Transform. i, 6–8
FIR	Finite Impulse Response. i, 6, 18
GPS	Global Positioning System. 2, 3
GUI	Graphical User Interface. 14
I/O	Input/Output. 12
IIR	Infinite Impulse Response. 6
IMU	Inertial Measurement Unit. 3, 9, 17
IP	Internet Protocol. 12, 15
IR	Infrared. 10
LADAR	Laser Detection And Ranging. i, v, 3, 4, 10, 11

LIDAR	Light Detection And Ranging. i, v, 3, 4, 10, 11
MAVLink	Micro Air Vehicle Link. 9
MSE	Mean Squared Error. iii, iv, 18, 25–27, 33
OS	Operating System. 12, 14
RADAR	Radio Detection And Ranging. i, 3, 4, 10, 11
RAM	Random Access Memory. 12
RTK	Real Time Kinematic. 1
SD	Secure Digital. 16
SDK	Software Development Kit. 11, 15
SONAR	Sound Navigation And Ranging. 3
TCP	Transmission Control Protocol. 12, 15
TOF	Time-of-Flight. 3, 4, 10, 11, 27
UART	Universal Asynchronous Receiver Transmitter. 11
UAV	Unmanned Aerial Vehicle. iii, 2, 9, 12, 16
USB	Universal Serial Bus. 10–12
VANT	*Veículo Aéreo Não Tripulado*. iv

List of Symbols

N	Number of samples. 18
μ_i	Average of the sensors at sample i. 18
ω	Frequency. 7
σ	Standard deviation. 18, 19, 23
MSE_M	Modified Mean Squared Error. 18, 23, 25–27, 33
c	Speed of light ($2{,}99 \times 10^9$ m/s). 4
d	Distance of the obstacle. 4
e	Euler number (2,71828). 18
e_i	Sensor error at sample i. 18
i	Sample index. 18, 19
t_r	Time of reception. 4
t_s	Time of sending. 4
w_i	Weight of the error at sample i. 18
x_i	Sensor reading at sample i. 18

1 Introduction

In agriculture, in general, the pulverization of fertilizers and pesticides is of prime importance. The use of manned aircraft is one of the most utilized methods for it due to the high speed of this approach, being able to cover big areas in short times. Its drawback is that for smaller areas such as farm borders or uneven geometries, the spraying is not feasible. For this scenarios, farmers usually resort to hand spraying (Spoorthi et al., 2017). A pulverization drone can be of great help due to its speed and accuracy. Also, as an advantage, the drone can automatically do the job without the need for human intervention.

Altitude sensing is a very important feature for any aircraft and can be helpful in collision avoidance and navigation. Aircraft of all kinds are usually equipped with barometric altimeters for this task. Specifically in a drone whose objective is to hover on low altitude, the ability to sense altitude precisely becomes mandatory. The lack of precision in the Height Above Ground Level (AGL) altitude can yield to severe consequences which include possibly losing the aircraft.

There are several challenges in altitude sensing in a crop environment. For instance, the inconsistency in plantation density can yield to places where ranging sensors stop detecting the top of the plants and start detecting the soil or somewhere in between. This can lead to misreading of the current altitude and consequently to unwanted disturbances in the altitude control of the aircraft. Another problem is related to the spraying process that generates droplets interfering with the readings either by being on the ray's range or by getting on the surface of the lens of optical sensors. Dust can be a challenge for optical sensors for the same reason being worsened by the turbulence generated by the rotors.

Another problem in the use of ranging sensors is the choice of the technology and of the sensor itself. The comparison between the sensors, even when there is data collected from them in a specific environment in not trivial as it requires relatively expensive equipment such as an Real Time Kinematic (RTK) or impractically big structures to guarantee a constant altitude above ground. Even with these complex systems, there can still exist the need for corrections related to topography.

In that perspective, this work's objective is to analyze and determine the best approach for altitude sensing in a variety of conditions. With the use of the measurements provided by more than one sensor, it is possible to calculate a more reliable reference to which the sensors can be compared. The real data acquisition from different environments combined with the proposed methodology supports the choice of the sensors and provides better decisions in the product's design.

This work is organized in the following sections: Theory Revision provides the introduction to the theoretical basis for this research. Materials describes the sensors used, as well as the drone and the board that collects the data from the sensors. Methods section presents the methodologies employed for the data acquisition and analysis. Finally, Results shows the data collected by the system, the filtering techniques' results and the final error calculations for each sensor in relation to the reference defined.

2 Theory Revision

This section presents a theory revision related to the pulverization process, altitude sensing for aerial vehicles and distance measurement techniques. It also includes a revision about digital signal processing tools.

2.1 Altitude Sensing

Autonomous estimation of the altitude of an UAV is extremely important when dealing with flight maneuvers like landing, steady flight, etc. (Cherian et al., 2009). When flying in low altitude, this measurement and its accuracy becomes vital for the aircraft. For this measurement, several approaches have been studied and used over the years.

The most common altitude sensing device present in almost any airborne system is a barometer based altimeter (Figure 1). Nelson, 1989 describes this sensor as "a sensitive pressure transducer that measures the ambient static pressure and displays an altitude value on the instrument dial" (p. 26). Still from the same author: "The altimeter is calibrated using the standard atmosphere and the altitude indicated by the instrument is referred to as the pressure altitude" (p. 26). One of the problems with this approach is that the pressure altitude and actual or geometric altitude will be the same only when the atmosphere through which the airplane is flying is identical to the standard atmosphere (Nelson, 1989). Another thing to consider is that this instrument measures Height Above Mean Sea Level (AMSL) and not AGL. This means that the AGL altitude needs to be estimated by using the takeoff altitude, either assuming that the area is perfectly leveled or using topography maps for estimating the ground altitude with respect to the mean sea level.

Altitude can also be estimated using Global Positioning System (GPS). However, standard GPS have a vertical precision between 25 meters and 50 meters and are sensitive to transmission interruptions in urban environment, for example (Eynard et al., 2010). Due to their lack of precision, these strategies would work assuming that most aircraft fly dozens of meters (usually more) above ground. However, for a pulverization drone or for any operation in low altitude, such as, take of and landing, a sensor that can measure AGL with error in the order of meters or less becomes necessary.

To face to this challenge, other methods for AGL altitude estimation were developed. Cherian et al., 2009 investigates the of use a single camera to accomplish this resorting to machine learning techniques. An evolution to this method is presented in Moore et al., 2010 and Eynard et al., 2010, using stereo vision camera to avoid the problems encountered by a single camera that most of the times lacks enough information to determine distances precisely. Moore et al., 2010 goes even further, being able to detect collisions in a cylinder around the aircraft due to the particular type of lenses and mirrors used in the vision system. Campbell and Blinn, 1968 develops methods for the estimation of the velocity/altitude ratio using two microwave passive sensors at different angles aligned in the same plane that sense the microwave emissions of the ground and calculate the said

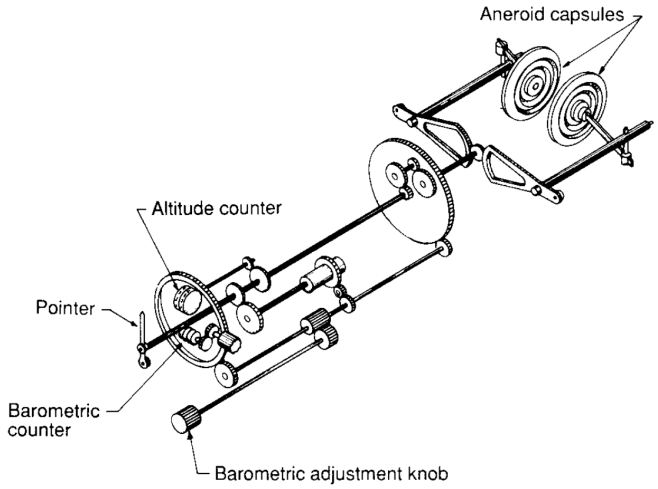

Figure 1: Pressure based altimeter found in most piloted aircraft.

Source: Nelson, 1989

ratio by using the time it takes for a point of measurement in the forward pointed beam to reach the backwards one.

The most widely used methods in commercial solutions though, are optical, RADAR or Sound Navigation And Ranging (SONAR) based, due to their operation simplicity and reliability. Since they do not require high processing power and are less likely to generate artifacts (compared to computer vision techniques), these systems are being adopted in a variety of applications. Cho et al., 2011 and Thomas et al., 2013 use RADAR altimetry fused with GPS and Inertial Measurement Unit (IMU) data to provide altitude sensing on takeoff and landing situations.

2.2 LIDAR and LADAR

LIDAR and LADAR technologies are very similar mainly because of their shared working principle (Figure 2). Depending on the source they can even be treated as a single technology often called just LIDAR. However, aiming to better characterize the differences between them, this work will differentiate them as LADAR for the laser based sensors and LIDAR for the regular ones. The primary function of LIDAR and LADAR sensors is to measure the distance between itself and objects in its field of view (LeddarTech, 2017c), thus characterizing a Time-of-Flight (TOF) sensor. It does so by calculating the time taken by a pulse of light to travel to an object and back to the sensor, based on the speed of light constant (LeddarTech, 2017c).The calculation made by this kind of sensor to provide the distance measurement is defined by equation (1),

$$d = \frac{c}{2}(t_r - t_s) \tag{1}$$

where d is the distance to the obstacle, c is the speed of light, t_r is the time of the reception and t_s is the time when the pulse was sent. The main difference between them is the divergence angle of the beam used. In LIDAR, the beam is much wider, providing a bigger coverage area but having some impact in the accuracy of the measurements. LADAR by the other hand, uses laser pulses, which have a much narrower beam with a much smaller divergence angle, meaning that the energy of the light pulse is concentrated in a much smaller area, yielding to better reflections and consequently, better accuracy (Sensorsinc, 2017).

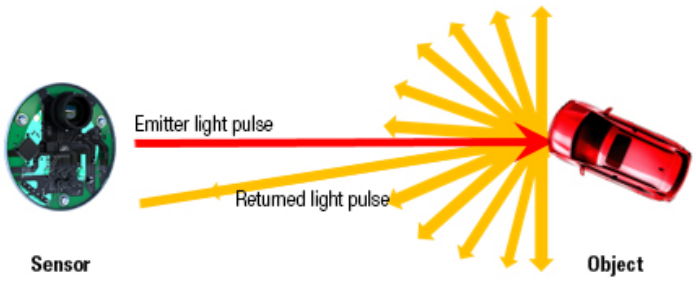

Figure 2: Working principle of LIDAR and LADAR.

Source: LeddarTech, 2017c

2.3 RADAR

A RADAR is a TOF sensing device that uses radio pulses instead of light for the ranging process. Although being similar to LIDAR and LADAR in its working principle, it differs significantly by using an electromagnetic wave with much bigger wavelength. This makes the RADAR more tolerant to small artifacts in its field of view. This way, it can provide robust performance in any weather condition (Aerotenna, 2017b) and environments with high suspense particles count. This technology is used worldwide in all kinds of applications, from weather forecast, using Doppler RADAR, to vehicles, where it can be used to provide spatial awareness in drive assist systems or in fully autonomous driving vehicles.

2.4 Crop Pulverization

The process of crop spraying is used worldwide in plague control for agriculture purposes. It consists of using pulverization devices to spread a certain type of pesticide or fertilizer to provide a better result for the harvest. This kind of production enhancement can provide increased productivity, improve quality and reduce costs significantly in large scale (Faiçal et al., 2014).

The most used techniques are manual or airborne with the use of piloted airplanes. Manual methods provide a more precise approach, being able to address only the correct areas, the drawback is that it needs loots of manpower, being a laborious task. Another disadvantage of the manual

spraying is the toxicity of the agrochemicals used. These are known to cause several diseases and problems to humans who have prolonged contact with it. One of the possible solutions to this problem is the use of special clothing and equipment to isolate the operators from the harmful material. Though, this reduces mobility and the productivity Aishwarya et al. (2015).

The airborne approach enables the coverage of much bigger areas at the price of a bigger waste because of not addressing only the necessary areas or due to the lack of accuracy and wind influence (Faiçal et al., 2014). Another problem, still related with the lack of precision of this technique is the harm that the pesticides can make in neighbour crops by the diffusion of it by the wind.

Ground based machines can be used for this purpose but this, in turn, provides other challenges. Namely, the irregular terrain and the height of the plants can be troubling for a grounded machine. Spraying trees, for example, is impossible when the agrochemicals need to reach the leaves. The pulverization drone comes as an effort to accomplish precision tasks with a higher efficiency, speed and lower labour necessities in adverse terrain conditions and in diverse plant heights. Figure 3 shows a pulverization drone in action.

Figure 3: Pulverization drone in action

Source: Skydrones Tecnologia Aviônica S/A

2.5 Digital Signal Processing

Digital signal processing is an area in computer science and signals that aims at the use of computing devices, such as computers, microcontrollers and Digital Signal Processor (DSP) to analyze and process signals that have been already converted to a digital form through the use of an Analog-Digital Converter (ADC). This can include a variety of fields like visual imagery enhancement, speech recognition and processing and sensorial data filtration (Smith, 2002).

2.5.1 FIR Filters

Digital filters use a digital processor to implement the action of filtering in a time signal. It does this by processing a sequence of discrete values to produce a new sequence of values that is the filtered signal. The FIR filter is an implementation that has linear phase, thus yielding to no phase distortion, an important characteristic when the timing of the signals matters. Also, when compared to a similarly specified Infinite Impulse Response (IIR) filter, the FIR will be longer, thus being more computationally demanding (Haykin and Venn, 2001). As this work will do the signal processing in an offline basis, this last characteristic could be neglected to improve the results of the filtration process because of the already stated phase characteristics of FIR filters.

In this kind of filter, an important parameter to be chosen is the window that will define the frequency response of it. The two most used windows are the Hamming and the rectangular, shown in Figure 4 with 50 coefficients.

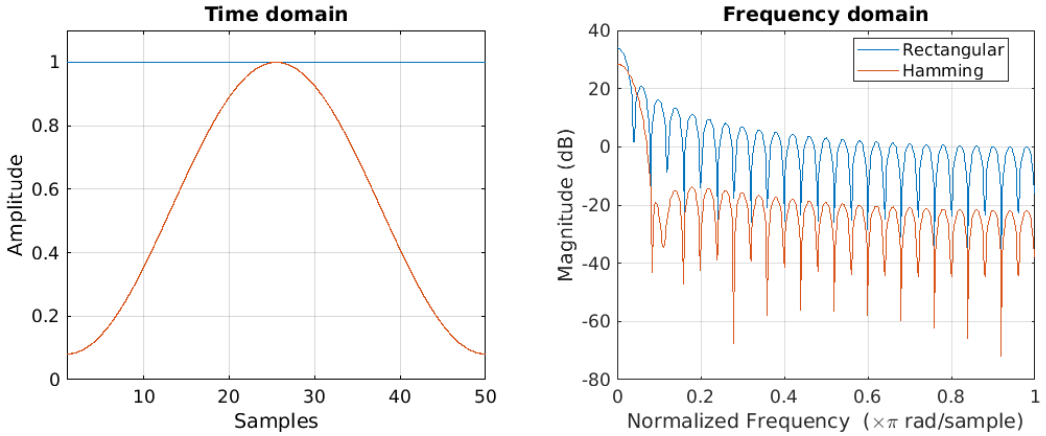

Figure 4: Hamming x Rectangular Comparison

Source: Author

The Hamming window has a wider transition region but has much lower oscillation amplitude in the side lobes, The rectangular window has a smaller transition region but oscillation amplitudes much higher in the side lobes caused by the ripple inserted when the window is truncated (Haykin and Venn, 2001).

2.5.2 FFT and Spectrograms

The Fourier Series representation was first developed in modern history by Leonhard Euler in 1748, and consists in the representation of periodic signals by the use of a linear combination of harmonically related sines and cosines. This and its correlated techniques (such as the Laplace Transform) are used in many fields in engineering and science to describe and treat signals and functions (Oppenheim et al., 1997).

The Fourier Transform is a generalization of the Fourier Series representation method, which can be used with non periodic signals. This is achieved by taking the period of the signal to infinity and substituting the sum of the series by an integral, due to the fact that the frequencies do not need to be integer multiples of the base one as in the Fourier Series representation. This yields to the Fourier Transform presented in equation (2),

$$\hat{f} = \mathscr{F}(f) = \frac{1}{\sqrt{2\pi}} \int_{-\infty}^{\infty} f(x) e^{-j\omega x} dx \tag{2}$$

where $j = \sqrt{-1}$ and ω is the frequency (Kreyszig, 2011).

The FFT is a computationally efficient implementation of the Discrete Time Fourier Transform (DTFT), which in turn is an adaptation of the Fourier Transform to discrete signals. This adaptation uses the concept of interpolating the sampled points of a function using the sum of trigonometric functions in discrete frequencies as shown in equation (3),

$$\hat{f_n} = Nc_n = \sum_{k=0}^{N-1} f(x_k) e^{-inx_k}, n = 0, 1, \cdots, N-1 \tag{3}$$

where N is the number of samples and c_n are the coefficients of the DTFT (Kreyszig, 2011; Haykin and Venn, 2001). The method for calculating the FFT divides this sum in to layers of progressively smaller portions using an interlaced decomposition, calculates the frequency contribution of them and, then, aggregates the results layer by layer as shown in Figure 5 (Smith, 2002).

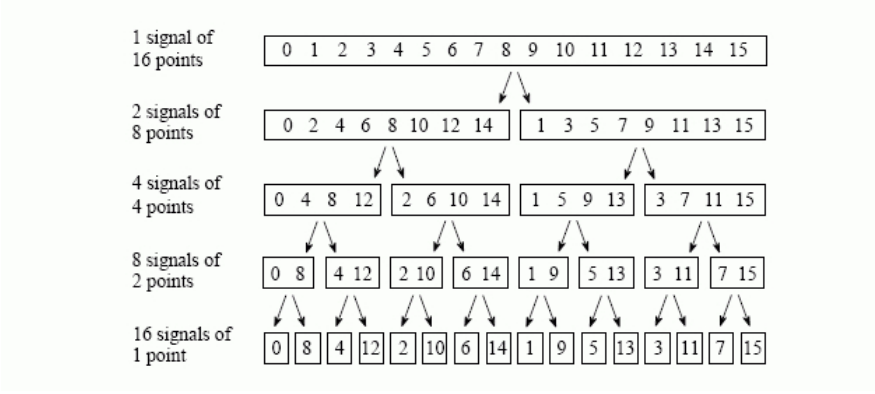

Figure 5: FFT Decomposition

Source: Smith, 2002

A widely used tool for visualization of Fourier Transforms is called the spectrogram. This technique is mostly used together with FFT because of its inherently high computational cost as it calculates the Fourier Transform of many time slices. The method works as follows: It is defined a

sample count for the FFT calculations and an overlap in number of samples, as well as the desired parameters for the FFT calculation itself. It is, then, calculated the Fourier Transform of each slice, accounting for the overlap, giving as a result, 2 dimensional matrix with the magnitude of a frequency in a given time slice in each cell. Then, this matrix can be graphically visualized with the help of color maps which map the magnitude to certain colors, yielding to plots like Figure 6.

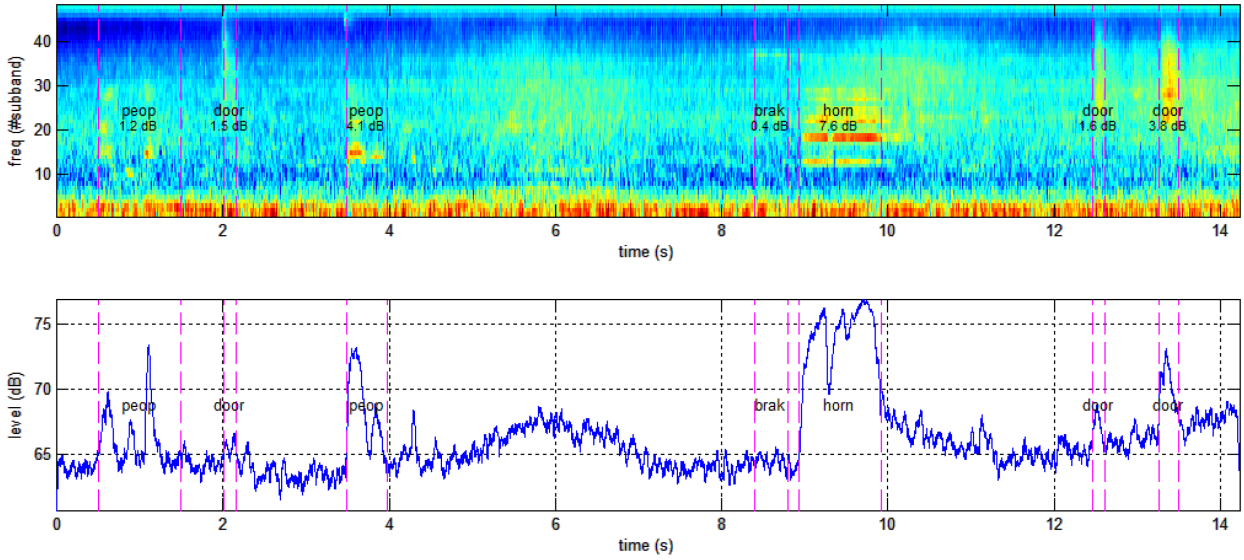

Figure 6: Example of use of spectrograms in sound analysis

Source: Alías and Socoró, 2017

This plot comes from a noise pollution analysis and shows how this tool can be useful to extract characteristics from a signal. In this example, the signal is a sound sample from Milan streets that is used for a noise pollution evaluation (Alías and Socoró, 2017).

3 Materials

This section describes the materials used to develop this research. The materials include all of the Commercial-Off-The-Shelf (COTS) hardware used as well as the additional parts developed during the work.

3.1 Pulverization Drone

The pulverization drone used in this research is a class 3 (ANAC, 2017) RPA Pelicano ®. This class is used for UAVs that weigth up to 25 kg. This aircraft has 8 rotors and can carry up to 0,008 m^3 (8 litters) or 10 kg of fluid to spray at a 0,000167 m^3/s (1 l/min) rate over a width of 4 to 5 meters (Skydrones, 2017). It flies between 1 and 3 meters over the crop and can cover up to 10000 m^2 (1 ha) per flight. The UAV can be seen in Figure 7.

Figure 7: Class 3 (ANAC, 2017) RPA Pelicano ®

Source: Skydrones, 2017

The Figure also shows the 6 pulverization sprinklers that distribute the fluid and the tank, which was removed to make room for the sensors' stand, which could, then be fixed to the carbon fiber tubular structure of the landing gear. The whole aircraft measures approximately 1,4 m in diameter and can be carried disassembled. The flight control is performed by a Pixhawk 2.4.6 Autopilot module, which comes with a 168 MHz Cortex M4F Central Processing Unit (CPU), an embedded 9 axis IMU (Accelerometer, Gyroscope and Magnetometer) and a barometer (Skydrones, 2017). This module can communicate to different modules and radios using the Micro Air Vehicle Link (MAVLink) Protocol.

3.2 Sensors

To provide the altitude readings in the required precision (in the order of tenths of meters), The alternative approached with this work is the use of distance TOF sensors. These are pointed downwards and measure the vertical distance between the drone and the plantation, vegetation or ground below it.

The sensors used in this work are different in many aspects. While all of them use electromagnetic waves to measure the distance between the drone and the soil, the range, acquisition rate, divergence angle and wavelength of them varies. Table 1 shows a synthesis of the characteristics of the sensors used in this study and was built with information from Optoelectronics, 2016, LeddarTech, 2017b, LeddarTech, 2015 and Aerotenna, 2017b. All of them were connected to the data acquisition board using Universal Serial Bus (USB), through adapters where needed.

Table 1: Sensor Specifications

Sensor	Lightware SF11-c	LeddarTech LeddarOne	LeddarTech M16	Aerotenna μLanding
Technology	LADAR	LIDAR	LIDAR	RADAR
# Rays	1	1	16	1
Aperture (°)	0,2	3	95	20 x 30
Sensing Rate (Hz)	20	140	1,56 - 100	800
Accuracy (m)	+- 0,1	0,05	+- 0,05	0,05
Resolution (m)	0,01	0,03	0,01	0,01
Min. Range (m)	0,1	0	0	0,32
Max. Range (m)	120	40	100	45
Interface	RS-232	Proprietary - USB	Proprietary - USB	RS-232
Wavelength (m)	905×10^{-9}	850×10^{-9}	940×10^{-9}	12.5×10^{-3}

Source: Author

The Lightware SF11-C (Figure 8a) excels in low refresh rate high precision measurements with a very narrow detection field due to the use of an Infrared (IR) LADAR to estimate distances. The Leddartech M16 (Figure 8c) and LeddarOne (Figure 8b) both use the same method to find range, the LIDAR technology, featuring a wider detection range than laser while still leveraging on IR to detect the distance between the sensor and an obstacle (in this case, the drone and the soil or the crop). These sensors are in the mid spectrum when it comes to refresh rates and differ from each other mainly by the aperture angle and the amount of rays (LeddarOne has one ray and M16 has 16 rays). Finally, the Aerotenna μLanding (Figure 8d) is the only sensor that uses microwave RADAR to detect obstacles. This sensor has the wider detection field with a 20° x 30° rectangular sensor. The resolution and accuracy parameters of these sensors are comparable, thus contributing to the fairness of the comparison in this work. It is important to note that the uncertainty and actual accuracy of each sensor individually is out of the scope of this research, being the comparison between them its real objective.

(a) Lightware SF11-C LADAR

Source: Optoelectronics, 2016

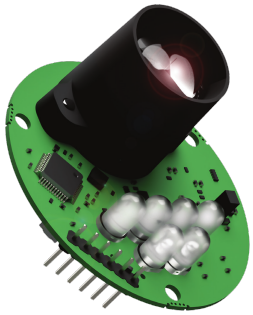

(b) LeddarTech LeddarOne LIDAR

Source: LeddarTech, 2017b

(c) LeddarTech M16 LIDAR

Source: LeddarTech, 2017a

(d) µLanding RADAR

Source: Aerotenna, 2017a

Figure 8: Sensors used in this study.

In terms of method for detection, all of the sensors use the time between the sending instant and the reflection receiving (TOF) to determine the distance between the emitter and the obstacle. While the method is the same, each sensor has different characteristics in terms of the sensitivity to different colours and textures in the obstacle being detected.

The communications between the sensors and the data acquisition board are done through various protocols, depending on the sensor. The Lightware sensor communicates via Universal Asynchronous Receiver Transmitter (UART) through the USB port in the sensor. The Aerotenna communicates also through UART but as it does not have any USB converter internally, an external board was used to get the signals through USB. Both the LeddarTech sensors use a proprietary Software Development Kit (SDK) to communicate with the sensors via USB so a software was

developed using the development kit to transmit the received data through Transmission Control Protocol (TCP)/Internet Protocol (IP) sockets to the data collecting software.

3.3 Data Acquisition Hardware

The hardware to which all of the sensors are connected is a Raspberry pi 2 B. This board has a 900 MHz quad-core ARM Cortex-A7 CPU, 1 GB Random Access Memory (RAM) and 4 USB ports that are going to be used to connect to the sensors (Raspberry Pi Foundation, 2017). The board runs a custom Linux kernel based operating system, which is a branch from Debian Operating System (OS) and is called Raspbian OS. During preliminary tests, this system showed enough performance to accomplish the desired data acquisitions without degrading the results by any means, being so, approved for the task. Figure 9 shows the Raspberry Pi 2 with the four USB ports used in this work and other Input/Output (I/O) that can be useful in future improvements.

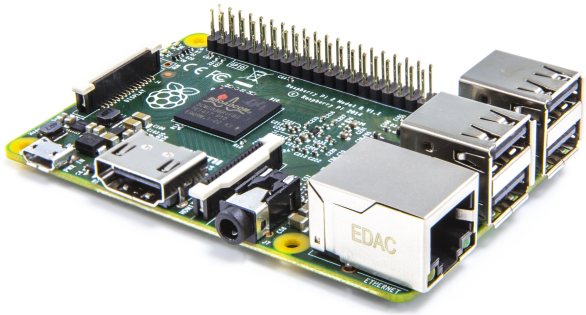

Figure 9: Data Collecting Hardware

Source: Raspberry Pi Foundation, 2017

A stand for all the sensors and data acquisition hardware was made to be carried by the drone. It was necessary to carry all of the sensors at once to make sure to be capturing their differences only and not any difference related to the path or altitude of the UAV during each pass over the crop. The stand itself can be seen in Figure 10. It was developed using Computer Aided Design (CAD) software taking into consideration the fixing method and the positions of the sensors to provide the correct alignment between the capture devices, thus, avoiding divergences caused by the pitch movement necessary to move the drone. Then it was manufactured in fiberglass using a CAD/Computer Aided Manufacturing (CAM) software and a Computer Numeric Control (CNC) milling machine.

In Figure 10, can be seen, from left to right, the Lightware sensor, the M16, the Aerotenna and the LeddarOne. The choice of the order was made to improve balancing of the structure around it's geometric center, thus having small influence in the balance of the carrying drone. The structure was fixed to the drone's landing gear using hooks in it designed to fit the soft foam cover of the

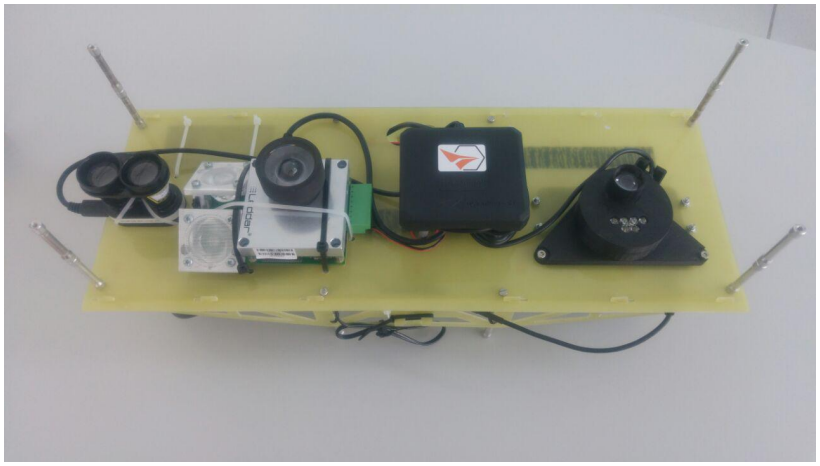

Figure 10: Stand for the sensors.

Source: Author

carbon fiber tubes that compose the landing gear. This structure mounted to the drone is shown in Figure 11.

Figure 11: Sensors in the pulverization drone

Source: Author

4 Methods

This section describes the methodologies used to collect, process and visualize the data. A description of the working principle of the software developed to collect the data needed for the analysis is also provided.

4.1 Data Acquisition

To gather the data coming from the sensors and handle the communications with them, a software was developed. The chosen language for it was Python since it would be running on a Raspberry pi 2 board running the Raspbian OS which is very tightly integrated with the hardware of the board and also with the language's packages. This way, the need for complex setups was avoided and also the programming task was simplified since it is a very efficient to write language and does not suffer from a big performance penalty.

The graphical interface developed for the software can be seen in Figure 12. The user can connect and disconnect to each of the sensors individually and see the data coming from each sensor in a graphical and also in a numerical way. The Graphical User Interface (GUI) provided also shows the maximum, minimum and average values for multi-ray sensors. It is possible to check the events log for deeper information on the running application and save the logged data to CSV files.

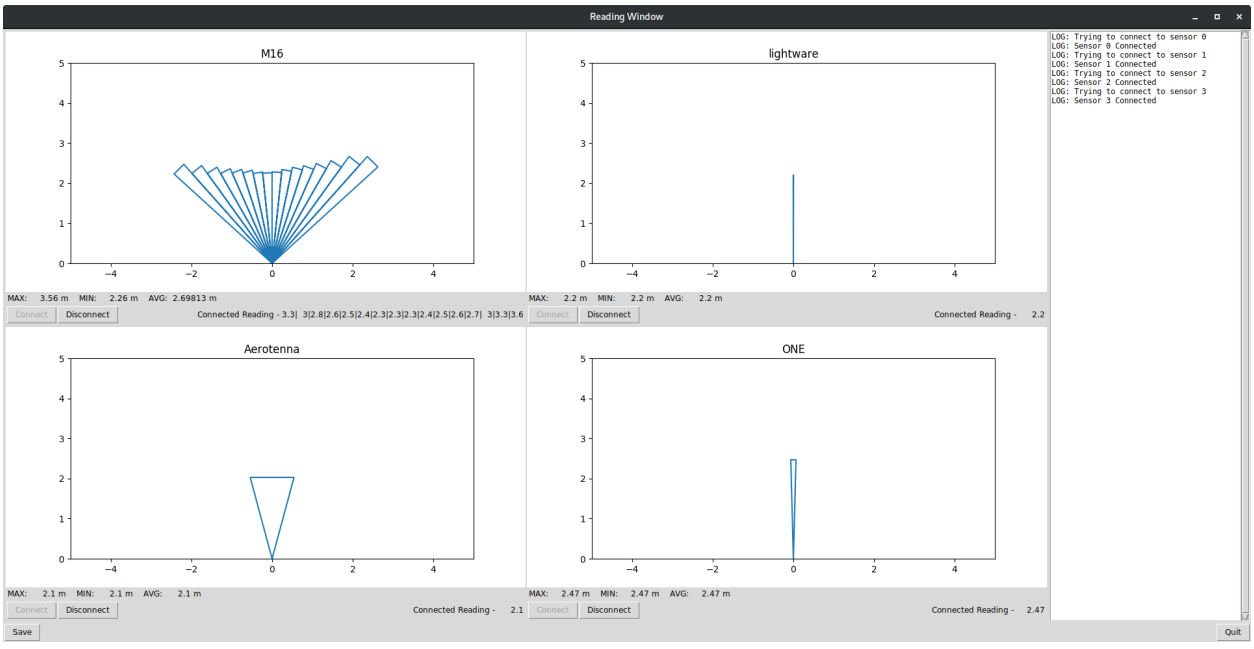

Figure 12: Data Collecting Software

Source: Author

The graph that illustrates the signals from the sensors, shows accurately the aperture angle and the ray geometry from the source to the detection. For sensors with more than one ray, the graph shows each ray in the correct direction. In this image, all of the sensors were pointed to the same flat surface and positioned at the same distance from it.

Two of the sensors, namely, the LeddarOne and the M16 needed the use of a proprietary SDK provided by the manufacturer to make the reading process and the setup possible. As this SDK is written in C language, a software using the proprietary pre-compiled functions provided to make the initial hardware configuration and make the readings was writen. This program sends, then, the live data to the data acquisition application through TCP/IP sockets.

At the start of the program, it asks the user to disconnect all the sensors so that it can initiate the recognition of each individual sensor. This had to be implemented since the ports in Linux systems are not static, meaning that the order of the connection of the sensors to the board influences the assignment of the ports to them. Also, it is not guaranteed that on a reboot, the ports will remain the same for each sensor.

The CSV structure of the files and the naming of them follows the one in the Figure 13, where "<filename>" refers to the name defined when saving and "<alias>" refers to the sensor's alias which can be seen in Table 2. The files can, then, be read separately or together using a spreadsheet editor or a numerical calculations application to analyze the collected data. The software also provides a very simple Command Line Interface (CLI) that can be used for minimum performance overhead and latency between reading and logging.

Figure 13: Naming and structure of the CSV file

Source: Author

Table 2: Sensor Aliases

Sensor	Alias
Lightware SF11-c	lightware
LeddarTech LeddarOne	One
LeddarTech M16	M16
Aerotenna μLanding	Aerotenna

Source: Author

The flight executed by the drone to capture the data was planned and the pilot was instructed

accordingly. The first guideline refers to the smoothness of the flight. The pilot was told to maintain the flight as stable and smooth as possible to simulate a self driven flight. The altitude should be kept at around 3 meters from the vegetation (as is usual in the pulverization process). Also, the aircraft should be controlled mostly by the pitch and yaw Degrees of Freedom (DOF) since these are the most relevant controls for the task, avoiding distortions caused by the position of the sensors related to the roll movements. Finally, the flight should include parts of smooth terrain and also parts with the environment being analyzed so as to enable the comparison to a surface known to cause little to no issues with the readings. The system starts recording with the drone on the ground and the data recorded includes the takeoff and landing processes. The data is, in the end of the flight, saved to an Secure Digital (SD) Card for further processing. A diagram showing the data acquisition process can be seen in Figure 14.

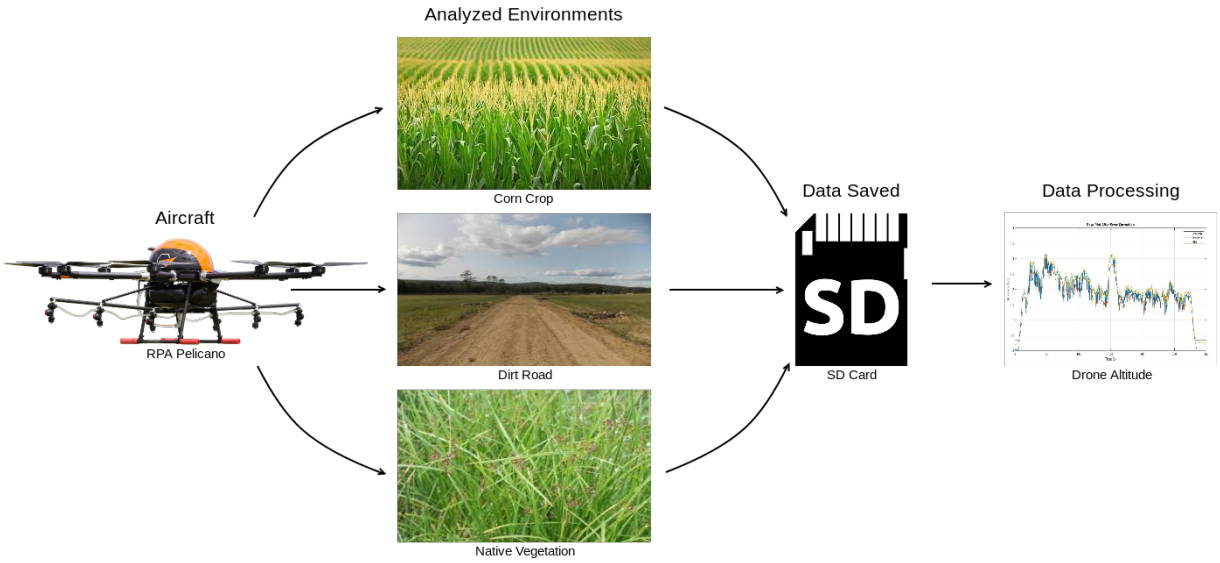

Figure 14: Data acquisition diagram

Source: Author

4.2 Ground Truth

In order to compare the four sensors described, a baseline should be set. At a first moment, the sensors on board the Pixhawk module were analyzed to determine their capability to provide an altitude baseline. For the purpose of measuring the altitude of the UAV, the system comes equipped with a barometer (MEAS MS5611). It can be seen when looking at its datasheet (TE Connectivity, 2017) that the rated resolution of the measurements is of 0,1 meters which is enough to accomplish the task of flying over the crop in a safe way without loosing much precision on the pulverization process. While testing the real precision of the pressure sensor, though, it shown results much worse than expected, having more than 1 meter of oscillation while sitting on a rigid surface. This

inaccuracy would be very bad for the task so, this sensor was discarded.

The other sensor capable of measuring altitude on board the Pixhawk is the IMU, however, it is known (Liu and Pang, 2017) that accelerometers (the main source for position estimation in this kind of unit) have poor performance for measuring absolute distances and tend to drift over time because of the errors in the double integration process, even when paired with Kalmann Filters. Seeing that, the solution found for estimating the ground truth for the altitude was a competitive system (Aishwarya et al., 2015).

The method consists of considering each sensor as an agent voting for an altitude. This technique is used in Artificial Intelligence (AI) (Aishwarya et al., 2015) and is usually based on discreet outputs from which each agent can choose. To be able to use this policy, it has to be modified so that it accepts continuous values. In this case, it was chosen to take the two closest values measured by the sensors and use the average of them as an altitude estimate. Considering that the sensors are very different and that all of them work well in a majority of the cases, this method should provide a good ground truth to compare the sensors to. Some further testing with adjustments to this technique to obtain better estimations were made and the results of are shown in the results section.

4.3 Analysis Methodology

The analysis process for the data collected followed the workflow displayed in Figure 15.

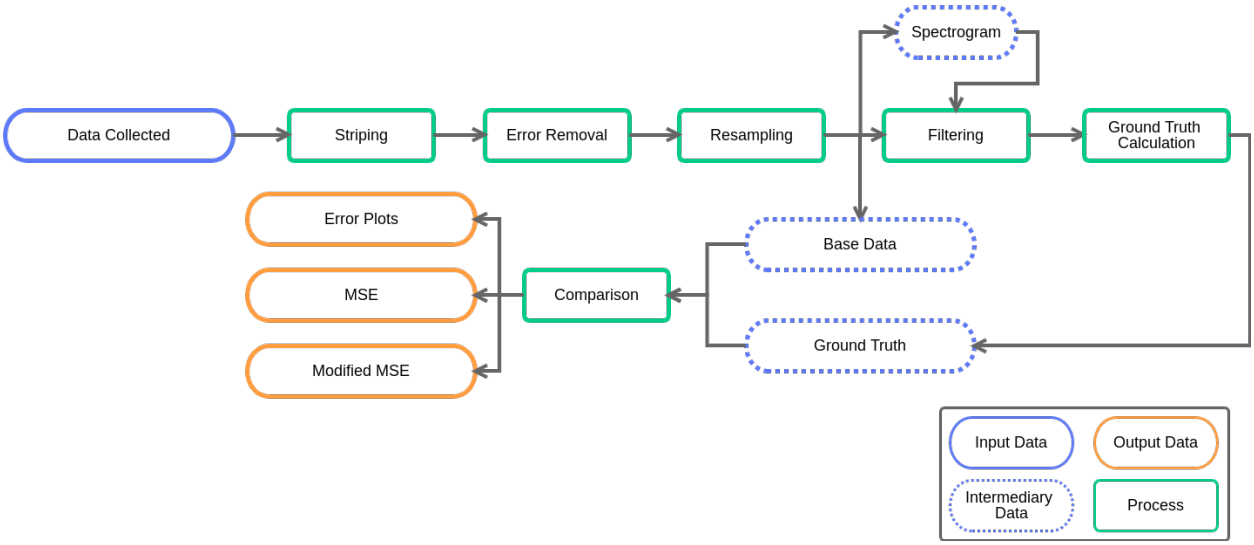

Figure 15: Analysis workflow

Source: Author

The first step in the analysis is to strip the unnecessary data, including ground time and manual positioning of the aircraft. This step is followed by an error removal algorithm that handles

communication and reading errors, using the reading limits of the sensors. Then, the signals provided by the slower sensors are resampled to 800 Hz using linear interpolation an anti-aliasing FIR filter. At this stage, the data from the sensors can be compared by their altitude data in a given sample. Next, to calculate the ground truth, the sensors have to be filtered, in an effort to reduce the vegetation interference in the value to which each sensor is going to be compared. To be able to do this, more information about the signals is necessary to chose the frequencies of the filter to be used, thus, spectrograms were built using data in regions with and without vegetation and were compared. The Matlab function filtfilt was used to filter the data with no phase modification. This feature is very important for the result as it is highly tied to the syncrony between the sensors and the ground truth calculated. This function accomplishes the zero phase filtering by passing the signal through the desired filter, reverting the samples and passing it again by the same filter, thus leading to the cancellation of the phase. Before the filtering stage, the ground truth is calculated using, at each sample, the average between the two sensors that are closer to each other and the standard deviation, that provides information about the dispersion of the data used. The resulting values are, then, passed through a filter with similar specifications to the one used for the the sensor data but with a lower stopband attenuation as this is used only to remove the discontinuities caused by the calculation methodology. The data is, then, manually tagged with the aid of a video recording of the flight, split in segments corresponding to the tags and used in the error calculation stage.

The error calculation stage consists of, first calculating the MSE of the segment of each sensor in relation to the ground truth calculated as depicted in equation (4),

$$\mathrm{MSE} = \frac{1}{N}\sum_{i=1}^{N}(x_i - \mu_i)^2 = \frac{1}{N}\sum_{i=1}^{N}(e_i)^2 \tag{4}$$

where MSE is the mean square error, N is the number of samples, i is the sample index, x_i is the sensor reading, μ_i is the average of the sensors in each sample and e_i is the error at each sample.

Then, to provide a better estimation of the error, using the data from the standard deviation of the ground truth, a modified version of the MSE is used as depicted in (5).

$$\mathrm{MSE_M} = \frac{1}{N}\sum_{i=1}^{N}(e_i w_i(e_i))^2 \tag{5}$$

Where $\mathrm{MSE_M}$ is the Modified Mean Squared Error and w_i is the weighting calculated for the given error. This error calculation function uses the standard deviation, to calculate the weight of the error. The weight calculation can be seen in equation(6),

$$w_i(e_i) = 1 - e^{-\frac{(e_i-\mu_i)^2}{2\sigma_i^2}} \tag{6}$$

where e is the Euler's number, μ_i is the average in sample i and σ is the standard deviation in

sample i and uses 1 minus a gaussian function to provide a low weight for the error when it is small and a weight of 1 when the error is big in relation to the standard deviation σ.

As the workflow shows, the data that is compared to the ground truth is taken right after the resampling stage. This is done to provide a comparison using the data provided by the sensor unfiltered, a situation closer to what would be the desired implementation. Since the filtfilt implementation is, by its nature, anti-causal, meaning that it cannot be implemented in an online basis, using the data filtered by it would not represent the actual result the sensors would give in a real application.

5 Results

The data was collected at the Agronomics Experimental Station of UFRGS. The flight made was over a corn crop and a native vegetation area as well as some regular terrain for reference.

The data acquisition process occurred in a day with high solar incidence and thus, yielded to some issues with the LeddarOne sensor. This sensors illuminators could not provide correct readings in this condition because of the solar reflections interference, thus leading to the elimination of this sensor from the analysis. It is important to say that in any moment in the laboratory, this sensor showed this kind of problem and that further testing was made altering the sensor's parameters (accumulation time, averaging and illumination power) but none of these solved the problem in high sun incidence environments.

Following the workflow presented in the methodology section, a flight was performed over the crop field. The flight started by a takeoff phase over a dirt road. The drone was, then, driven to the crop and measured data from it, flying over plantation gaps and service corridors. The culture in use in this part of the data was corn with approximately 40 days, measuring 0,5 meters in average. The aircraft flies, then over the dirt road and follows to a native vegetation area. This area can be separated in two regions, one of them with heights of approximately 0,3 meters and a higher area with heights of approximately 0,8 meters. The data collected during this experiment can be seen in Figure 16 which shows the altitude measured by the three sensors versus time.

Figure 16: Raw data after error correction

Source: Author

In Figure 16, it can be seen that the takeoff phase takes about 10 seconds (from 6 to 16 seconds approximately). The corn crop phase goes from 15 seconds to 166 seconds approximately and includes many passages over gaps and service corridors. The flight part over the road goes from

147 to 154 seconds, presenting mostly a smooth surface similar to the one captured in the takeoff phase, and the native vegetation pass goes from 154 seconds to 269 seconds and presents a mixture of low and high plants, adequately tagged. Table 4 on Appendix C provides the timestamps for each kind of environment. These table was built using a video recording of the whole flight to tag the time markers approximately and then comparing them to the data from the sensors. At this stage, the Lightware sensor data was crucial as this sensor has a very narrow aperture, thus being highly susceptible to variation due to the texture of the surface under it. This provided a very clear indication of the accurate timings of the timestamps. Some of the tagged time periods can be seen in Figure 17. The selected time slices shown in this Figure will be used along the work to provide a step by step comparison

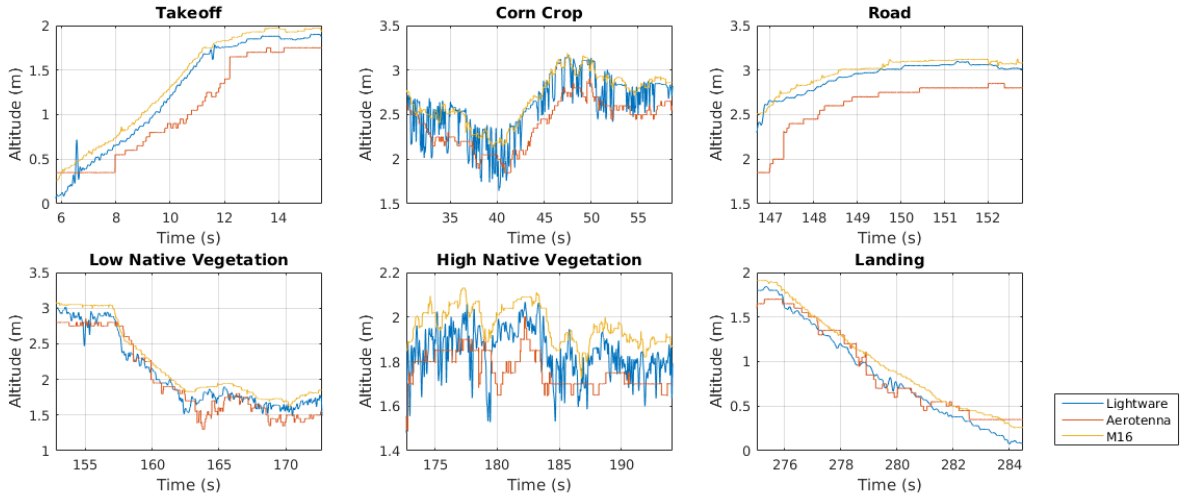

Figure 17: Timestamps zoomed

Source: Author

The plot extracted from the takeoff phase shows, as expected by the smoothness of the surface, a soft ascendance on all three sensors. The corn crop extract (mainly the Lightware sensor data) clearly shows a high frequency signal overlapped with a lower frequency one. The lower frequency signal is approximately the real altitude over the plantation, while the higher frequency signal represents the texture underneath, showing accurately variations with amplitudes close to the measurements of the plants. The road and Landing flight phases show similar results to the takeoff phase. The Native Vegetation phases do not show results as bad as the crop phase, probably because of the higher density of the plants but there is a clear difference in the amplitude of the oscillations between the high and the low native vegetation.

These observations were crucial to the further development of the analysis as they showed clear differences between the flight phases that can be easily recognized and characterized. To improve the understanding of the signals collected and to provide a better visual insight of the frequency content of the data, spectrograms of the 3 sensors under two separate conditions were built, during

takeoff and over the corn crop. These plots made possible to determine the best frequency for the filter to be used in the ground truth calculation. One of these plots can be seen in Figure 18, while the other two can be found in the Appendix A section. These kind of plots were used as an attempt to provide a good visualization of the spectral content of the signals in time and with them it was possible to see in smaller time divisions, the effect of specific phenomena. For instance, from Figure 18, it can be seen that the frequency content present in different time slices of the measurement is very different and that using the Fourier Transform alone in the whole signal from the corn crop could lead to misreading of the real contribution of the higher frequencies in the signal. This would be due to the averaging of regions that do not present the oscillations with the ones that present it. This, consequently would lead to a reduction of the magnitude of the higher frequency components in the measurement with respect to the lower frequency signal (of interest), making it harder to perceive.

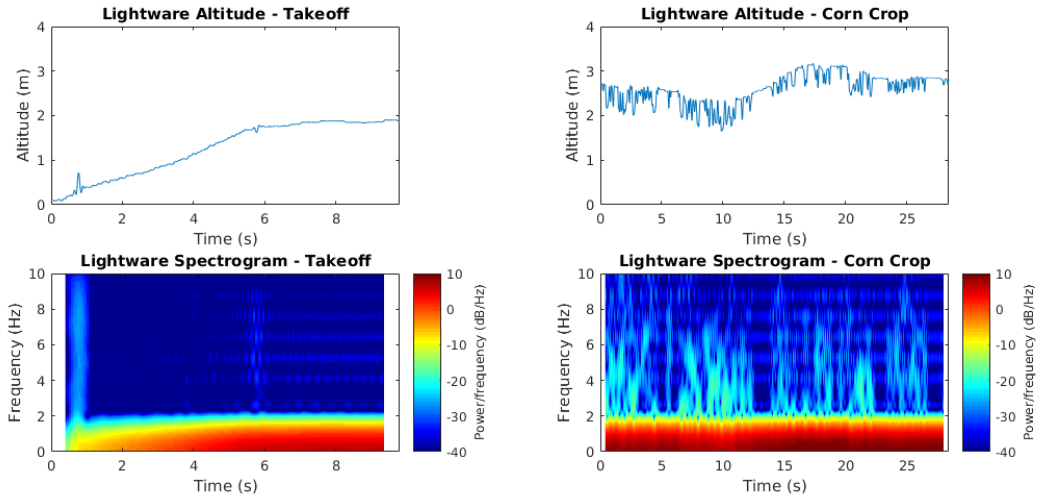

Figure 18: Spectrogram - Lightware

Source: Author

The altitude data followed by the spectrogram for the period of time is shown in Figure 18. On the left the data comes from the takeoff process, which took place at a very smooth surface, thus yielding to a clean signal that can be seen as a target for the filtration process. In these spectrograms, it can be seen that most of the power of the signal and, thus, most of the information of the signal is present below 2 Hz. On the right, the data comes from the section of the flight when the drone was over the crop. In this case, it can be seen that it is a signal with a much higher power in higher frequencies, as expected. Again, this is most prominent in the Lightware data. It can also be noted that around 1,5 Hz the spectrogram starts to be distorted by the crop.

Using these observations and after some fine tuning of the filtered results, a lowpass filter with a passband of 0.5 Hz, a stopbad of 1 Hz was chosen. To avoid having distortions caused by excessive attenuation in the region of interest, the passband attenuation selected was 0.01 dB. The stopband

attenuation selected was 100 dB. The window used by the filter was the Hamming window as it provides better attenuation of the side lobes, and thus, lower oscillation on the frequency response. These benefits come at the cost of a higher order filter to match the specifications. As this is an offline study and the computational power necessary for the calculations was enough not to slow down the analysis by a significant amount, this drawback could be neglected. Figure 19 shows a comparison between the original sensor data and the filtered data.

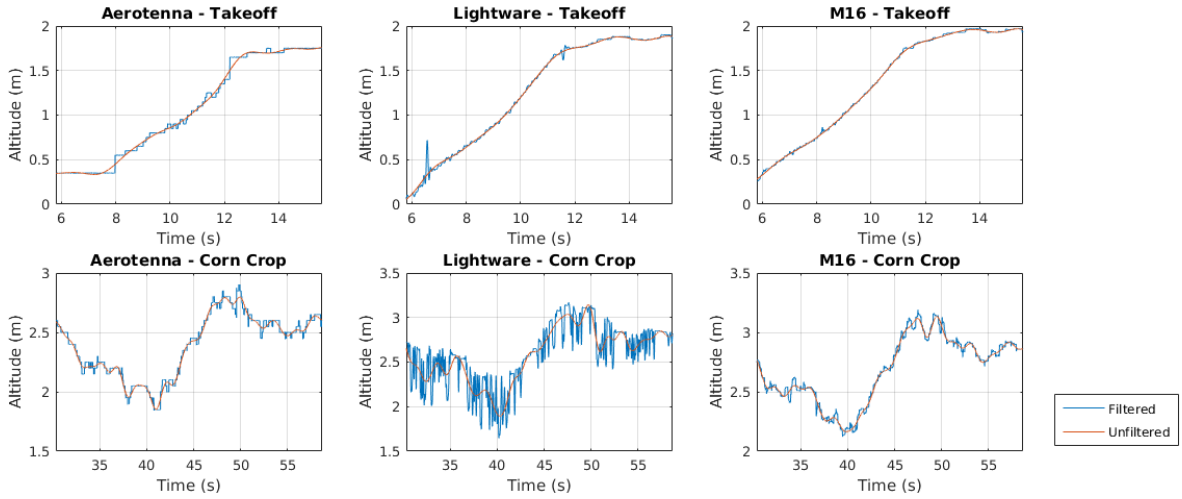

Figure 19: Comparison between filtered and unfiltered data.

Source: Author

In Figure 19, it can be seen that the data from the smooth takeoff process was not modified by much, while the data from the corn crop is much cleaner, showing little influence from the texture on the ground. An observation can be made about the altitude in the corn crop phase, mainly in the Lightware sensor data. The desired altitude to be measured would be the bottom of the negative peaks as this is the altitude with relation to the plants under the drone. In this sense, this filtration enhances the results, but further improvements could be made to provide a result closer to the desired. Also, what can be noted is that the magnitude of the signals remained mostly unchanged and there was no visible delay introduced by the filtration process.

The results from the last step could, this way be used to calculate the reference through which the sensors would be compared, the ground truth. This was, then calculated by the method described in the Methodology section, using the polling system and averaging the two closest results. Still at this stage, the standard deviation σ could be calculated from the two nearest sensors at each time point. This calculation was stored for the MSE_M calculation stage.

The resulting signal can be plotted against the filtered data from the sensors to ensure the coherence of the result and also, to provide a preliminary insight of the probable results to come from the error calculation. The plot can be seen in Figure 20 with the ground truth represented by a dashed line to improve readability.

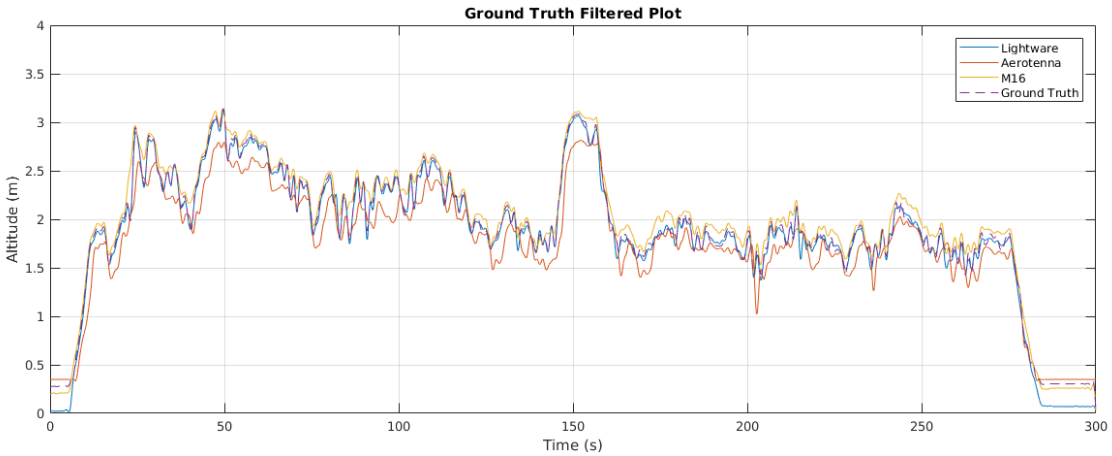

Figure 20: Ground Truth

Source: Author

Already shown in Figure 20, the ground truth calculation process is made correctly and provides coherent results. The reference calculated is seen between the sensors in all time points and follows the closest sensors. To enhance the visualization and provide a comparison to the raw data, plots of some of the tagged regions were made. These plots can be seen in Figure 21.

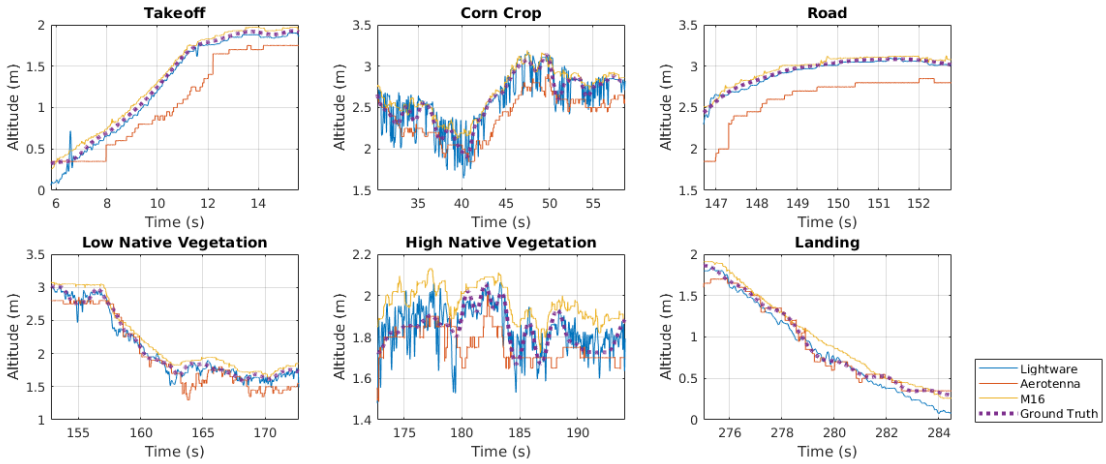

Figure 21: Ground Truth zoom

Source: Author

Figures 20 and 21 show the calculated truth to be a smooth curve that stays between the two closer sensors to each other, as designed. The effect of the filtering used to smooth the discontinuities alters the signal in a very subtle way, thus having very little influence in the end result.

At this stage, the error plots for each sensor can be displayed to provide a graphical visualization

of the accuracy of them with respect to the reference set by the ground truth. The error obtained for each sensor by subtracting its signal to the ground truth is displayed in Figure 25 in the Appendix B and some of the tagged periods are shown in Figure 22.

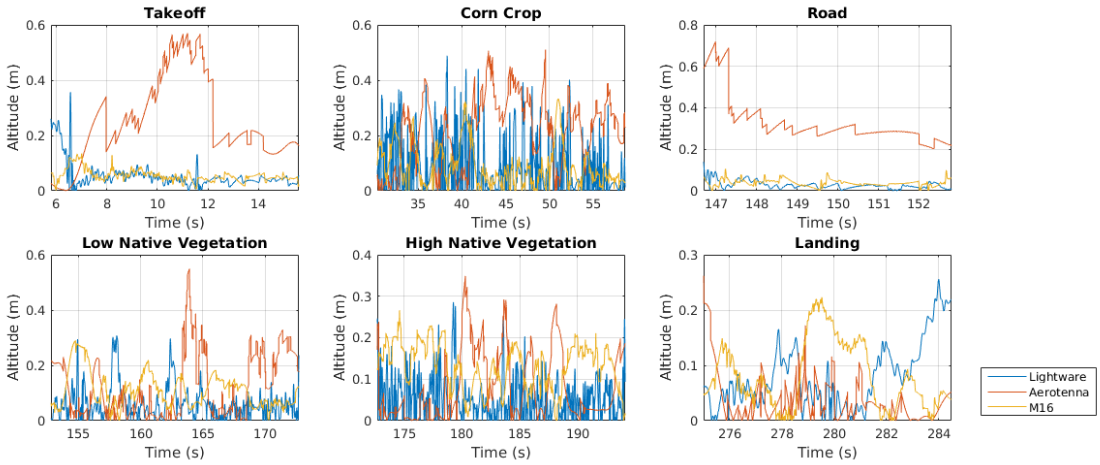

Figure 22: Error Plot Zoomed

Source: Author

Figure 22 already shows a trend where the Aerotenna sensor usually has the biggest error (around 0,3 to 0,4 meters in most cases). This is probably due to its lack of accuracy when compared to the optical sensors (Lightware and M16). These two sensors, by the other hand show errors of less than 0.2 meters in most scenarios. This error is considered to be acceptable considering the method used for estimation of the real altitude and the characteristics of the spraying process.

Table 4 in Appendix C shows the MSE and MSE_M in the timestamps tagged. In this table, the lower the value of the MSE or of the MSE_M, the smaller the overall error. To enable a better visualization of the data and knowing that crop gaps and service corridors are always part of the plantation, a table accounting for this fact, summarizing the areas of flight and recalculating the MSE's was built and is shown in Table 3.

Table 3: Error Summary

		MSE (m^2)			MSE_M (m^2)		
Duration (s)	Flight Phase	Aerotenna	Lightware	M16	Aerotenna	Lightware	M16
31,4	Smooth Ground	0,0553	0,0052	0,0063	0,0518	0,0036	0,0038
131,1	Corn Crop	0,0564	0,0177	0,0144	0,0531	0,0147	0,0108
86,6	High Native Vegetation	0,0256	0,0089	0,0176	0,0211	0,0066	0,0136
29,6	Low Native Vegetation	0,0344	0,0054	0,0127	0,0295	0,0033	0,0091

Source: Author

Table 3 shows that for situations where either the surface below the drone is smooth or the vegetation is dense enough, Lightware excels as the most overall accurate. In the other hand, the M16 is the most capable sensor on situations with many gaps and sparse vegetation, even without the use of more than one ray in the calculations. The Aerotenna sensor has the worse (bigger) MSE and Modified MSE indices in all of the cases. While in use in the laboratory, in fact, this was the most inaccurate of the sensors for static obstacles. This suggests that a process of determination of the static error of it and, possibly, magnitude adjustments in the signal provided by it, could be used to improve this sensor's results.

The MSE_M in Table 3 shown a similar result to the one seen in the MSE method. However, it can be seen that for results that are visibly closer in plots such as Figure 22, the MSE_M provides a better notion of the similarity of the sensing quality provided by the sensors. This is done while still keeping the distance of already distant signals, as shown in the takeoff section. In this time slice, for the Aerotenna, which performs the worse, the MSE_M shows results that are very close to the MSE, while the values for Lightware and M16 are much closer to each other, which matches with the visual perception of the data from this timestamp. This way, the MSE_M can be used more effectively when deciding the right sensor for each task as it is able to provide a better differentiation of the qualities and similarities of the sensors.

6 Conclusion

In airborne pulverization, it is essential to precisely measure the altitude of the aircraft, due to the obstacles present in the flight environment. In this sense, this work approaches the problem of altitude sensing by comparing different TOF sensors with different measuring technologies. This is done by collecting data from the sensors in a same flight and, then, developing a reference to which they can be compared. A baseline to which the sensors can be compared was developed by the use of signal filtration and a competitive algorithm and, in the end, metrics built around MSE and a modification of it are used as a basis to the decision making process.

One of the sensors used in the premature stages of this study showed unexpected issues with the environmental conditions in which the system needs to operate and was, this way, discarded. The other three sensors used presented good raw results.Through the described techniques, it was possible to develop a trustworthy baseline, which, while imperfect, represents a good approximation of the real altitude of the drone with respect to the crop. The error measurement techniques explored in this work presented coherent results to the expectancy and performed well enough to provide the data necessary to the decision making process.

The results shown that the Leddartech M16 and the Lightware SF11-C both perform well in different situations. The Lightware sensor excels in dense vegetation environments because of it's superior accuracy. The much narrower divergence angle shown not to be a problem in these environments as it is harder to penetrate through the leaf thickets. The M16 is the best choice in sparser vegetation due to it's bigger divergence angle, which captures a better averaging of the surface underneath. Additionally, its less precise measurements when compared to Lightware affect very subtly the overall performance of it as the MSE_M of the smooth ground measurements shown. This contributes to the choice of the Leddartech M16 as the best overall performer between the studied sensors, presenting the best results in most cases and in the exception cases, very similar measurements.

This study can be expanded and continued in a variety of forms. Namely, the use of the same workflow in different cultures can be of great help to improve the data basis. Different environmental characteristics can still be evaluated, including the weather conditions. The influence of the suspended particles and droplets caused by the rotors of the drone and the spraying fluids needs to be analyzed quantitatively (in relation to the numerical results), but also, qualitatively, with relation to the need for maintenance and the frequency of it caused by this conditions. Improvements could be done by adding more sensors to the study, which would increase the choice basis size and also could provide improvements to the competitive system used to calculate the ground truth, by increasing the number of competing agents. Also, of great importance, would be studies related to the collision avoidance during flight using the data from the sensors already present in this work or others.

7 References

Aerotenna, 2017a. MICROWAVE SENSORS.
URL https://aerotenna.com/sensors/{#}ulanding

Aerotenna, 2017b. Why μLanding?
URL https://aerotenna.readme.io/docs/why-μlanding

Aishwarya, B. B., Archana, G., Umayal, C., 2015. Agriculture robotic vehicle based pesticide sprayer with efficiency optimization. Proceedings - 2015 IEEE International Conference on Technological Innovations in ICT for Agriculture and Rural Development, TIAR 2015 (Tiar), 59–65.

Alías, F., Socoró, J., 2017. Description of Anomalous Noise Events for Reliable Dynamic Traffic Noise Mapping in Real-Life Urban and Suburban Soundscapes. Applied Sciences 7 (2), 146.
URL http://www.mdpi.com/2076-3417/7/2/146

ANAC, 2017. Regras Sobre Drones - ANAC (61).
URL http://www.anac.gov.br/noticias/2017/regras-da-anac-para-uso-de-drones-entram-em-vigor/release{_}drone.pdf

Campbell, J. P., Blinn, J. C., 1968. Experimental Evaluation of Passive Microwave Velocity/Altitude Sensing (July).
URL http://ieeexplore.ieee.org/stamp/stamp.jsp?arnumber=05409032

Cherian, A., Andersh, J., Morellas, V., Papanikolopoulos, N., Mettler, B., 2009. Autonomous altitude estimation of a UAV using a single onboard camera. 2009 IEEE/RSJ International Conference on Intelligent Robots and Systems, IROS 2009, 3900–3905.
URL http://ieeexplore.ieee.org/stamp/stamp.jsp?arnumber=05354307

Cho, A., Kang, Y.-S., Park, B.-J., Yoo, C.-S., Koo, S.-O., 2011. Altitude integration of radar altimeter and GPS/INS for automatic takeoff and landing of a UAV. International Conference on Control, Automation and Systems, 1429–1432.
URL http://ieeexplore.ieee.org/stamp/stamp.jsp?arnumber=06106153

Eynard, D., Vasseur, P., Demonceaux, C., Frémont, V., 2010. UAV altitude estimation by mixed stereoscopic vision. IEEE/RSJ 2010 International Conference on Intelligent Robots and Systems, IROS 2010 - Conference Proceedings, 646–651.
URL http://ieeexplore.ieee.org/stamp/stamp.jsp?arnumber=05652254

Faiçal, B. S., Pessin, G., Filho, G. P. R., Furquim, G., de Carvalho, A. C. P. L. F., Ueyama, J., 2014. Fine-tuning of UAV control rules for spraying pesticides on crop fields. In: 2014 IEEE 26th International Conference on Tools with Artificial Intelligence. pp. 527–533.
URL http://ieeexplore.ieee.org/stamp/stamp.jsp?arnumber=06984521

Haykin, S., Venn, B. V., 2001. Sinais e sistemas.
URL https://books.google.com.br/books?id=tdNYclZwaYIC

Kreyszig, E., 2011. Advanced Engineering Mathematics, 10th Edition.

LeddarTech, 2015. Leddar Sensor Module User Guide.

LeddarTech, 2017a. Leddar M16 16-Segment Solid-State LiDAR Sensor Module.
URL http://leddartech.com/modules/m16-multi-element-sensor-module/

LeddarTech, 2017b. Leddar One Fact Sheet.
URL http://leddartech.com/app/uploads/dlm{_}uploads/2016/09/SpecSheets-LeddarOne-290517-web.pdf

LeddarTech, 2017c. LeddarTech - Technology Fundamentals.
URL https://leddartech.com/technology-fundamentals/

Liu, H., Pang, G., 2017. Accelerometer for Mobile Robot Positioning.
URL http://biorobotics.ri.cmu.edu/papers/sbp{_}papers/integrated4/liu{_}accel{_}position.pdf

Moore, R. J. D., Thurrowgood, S., Bland, D., Soccol, D., Srinivasan, M. V., 2010. UAV altitude and attitude stabilisation using a coaxial stereo vision system. Proceedings - IEEE International Conference on Robotics and Automation, 29–34.
URL http://ieeexplore.ieee.org/stamp/stamp.jsp?arnumber=05509465

Nelson, R. C., 1989. Flight Stability and Automatic Control.

Oppenheim, A. V., Willsky, A. S., Nawab, S. H., 1997. Signals and Systems, 2nd Edition.

Optoelectronics, L., 2016. SF11 Laser Altimeter Product Manual.
URL http://www.lightware.co.za/shop2017/download/Documents/SF11-LaserAltimeterManual-Rev5.pdf

Raspberry Pi Foundation, 2017. Raspberry Pi.
URL https://www.raspberrypi.org/

Sensorsinc, 2017. Sensors Unlimited - LADAR.
URL http://www.sensorsinc.com/applications/military/ladar

Skydrones, 2017. Pelicano.
URL https://skydrones.com.br/pelicano/

Smith, S. W., 2002. The Scientist and Engineer's Guide to Digital Signal Processing.
URL http://www.dspguide.com/pdfbook.htm

Spoorthi, S., Shadaksharappa, B., Suraj, S., Manasa, V. K., 2017. Freyr drone: pesticide/fertilizers

spraying drone an agricultural approach, 252–255.
URL http://ieeexplore.ieee.org/stamp/stamp.jsp?arnumber=07972289

TE Connectivity, 2017. MS5611-01BA03.
URL http://www.te.com/commerce/DocumentDelivery/DDEController?Action=srchrtrv{&}DocNm=MS5611-01BA03{&}DocType=Data+Sheet{&}DocLang=English

Thomas, L., Monin, A., Mouyon, P., Houberdon, N. E. D., 2013. Gaussian mixture filtering for data fusion with switching observation models: Application to aircraft relative altimetry. Conference on Control and Fault-Tolerant Systems, SysTol, 294–299.
URL http://ieeexplore.ieee.org/stamp/stamp.jsp?arnumber=06693932

Appendices

Appendix A: Spectrograms

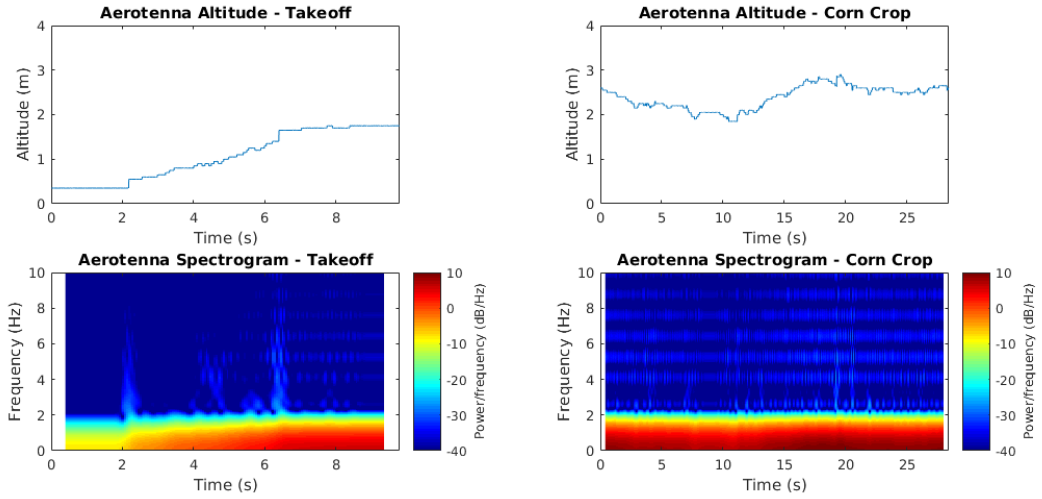

Figure 23: Spectrogram - Aerotenna

Source: Author

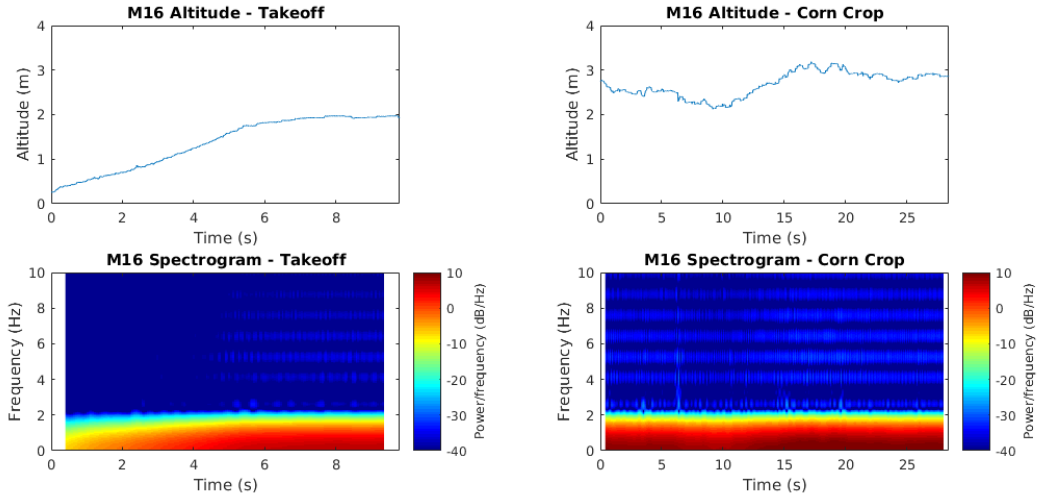

Figure 24: Spectrogram - M16

Source: Author

Appendix B: Error plot

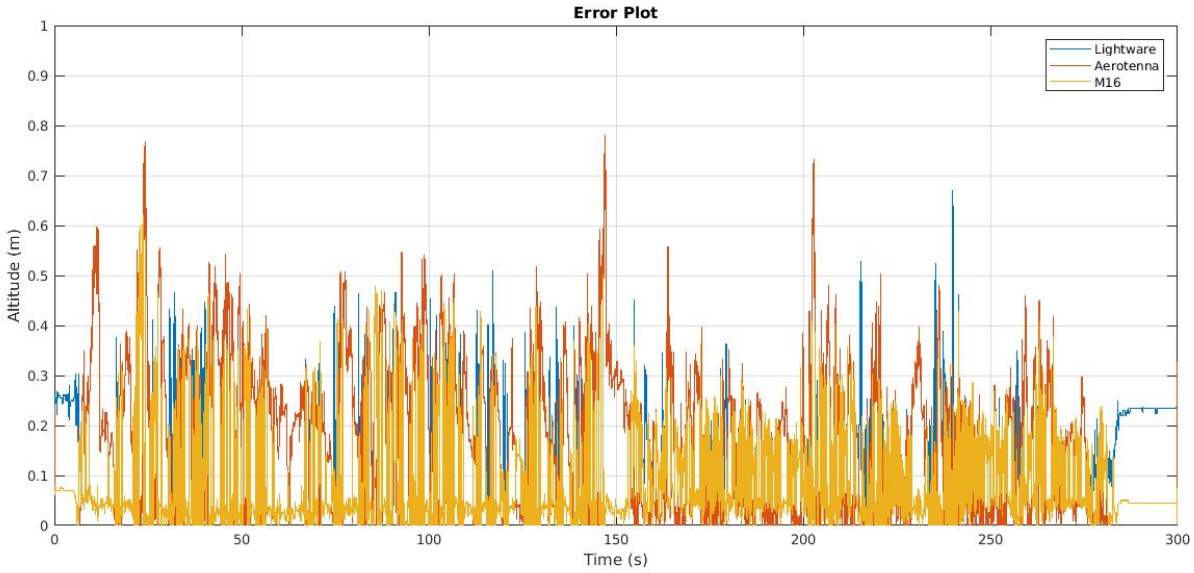

Figure 25: Error Plot

Source: Author

Appendix C: Data tagging and error results

Table 4: Error by tagged segment

			MSE (m^2)			MSE_M (m^2)		
Start Time (s)	Duration (s)	Flight Phase	Aerotenna	Lightware	M16	Aerotenna	Lightware	M16
5,8	9,8	Takeoff	0,0849	0,0053	0,0035	0,0790	0,0034	0,0007
15,6	2,5	Corn Crop	0,0277	0,0110	0,0066	0,0244	0,0088	0,0042
18,1	2,7	Small Gap	0,0836	0,0016	0,0023	0,0825	0,0000	0,0001
20,8	7	Corn Crop	0,0809	0,0201	0,0613	0,0697	0,0132	0,0512
27,8	2,5	Small Gap	0,1200	0,0035	0,0034	0,1192	0,0025	0,0005
30,3	28,4	Corn Crop	0,0628	0,0204	0,0133	0,0594	0,0170	0,0092
58,7	7,2	Big Gap	0,0385	0,0005	0,0012	0,0381	0,0000	0,0001
65,9	5,5	Corn Crop	0,0219	0,0158	0,0202	0,0183	0,0127	0,0155
71,4	3,2	Small Gap	0,0212	0,0016	0,0050	0,0183	0,0005	0,0020
74,6	39,3	Corn Crop	0,0606	0,0223	0,0176	0,0572	0,0191	0,0142
113,9	1,7	Small Gap	0,0650	0,0038	0,0055	0,0638	0,0020	0,0027
115,6	2,4	Corn Crop	0,0186	0,0385	0,0107	0,0152	0,0352	0,0076
118	1,9	Small Gap	0,0319	0,0009	0,0044	0,0306	0,0002	0,0027
119,9	26,8	Corn Crop	0,0519	0,0182	0,0070	0,0493	0,0155	0,0038
146,7	6,1	Road	0,1213	0,0011	0,0017	0,1212	0,0001	0,0002
152,8	19,9	Low Native Vegetation	0,0285	0,0071	0,0159	0,0232	0,0048	0,0121
172,7	21,4	High Native Vegetation	0,0137	0,0057	0,0197	0,0094	0,0036	0,0158
194,1	2,6	Low Native Vegetation	0,0365	0,0015	0,0039	0,0315	0,0000	0,0007
196,7	31,9	High Native Vegetation	0,0355	0,0094	0,0144	0,0307	0,0067	0,0103
228,6	4,9	Low Native Vegetation	0,0626	0,0016	0,0030	0,0609	0,0004	0,0010
233,5	33,3	High Native Vegetation	0,0238	0,0106	0,0192	0,0196	0,0084	0,0154
266,8	2,2	Low Native Vegetation	0,0225	0,0035	0,0159	0,0143	0,0003	0,0097
269	6	Plowed Land	0,0224	0,0020	0,0096	0,0154	0,0001	0,0051
275	9,5	Landing	0,0032	0,0098	0,0101	0,0021	0,0083	0,0084

Source: Author